



Article

Evaluation of Backscattering Models and Support Vector Machine for the Retrieval of Bare Soil Moisture from Sentinel-1 Data

Jamal Ezzahar ^{1,2,*} , Nadia Ouadi ³, Mehrez Zribi ⁴ , Jamal Elfarkh ⁵, Ghizlane Aouade ⁵, Said Khabba ^{2,3}, Salah Er-Raki ^{2,5} , Abdelghani Chehbouni ^{2,4} and Lionel Jarlan ⁴ 

¹ Ecole Nationale des Sciences Appliquées, Université Cadi Ayyad, Safi B.P. 511-40000, Morocco

² Center for Remote Sensing Application (CRSA), Mohammed VI Polytechnic University, Ben Guerir 43150, Morocco; khabba@uca.ac.ma (S.K.); s.erraki@uca.ma (S.E.-R.); ghani.chehbouni@ird.fr (A.C.)

³ Faculté des Sciences Semlalia, Université Cadi Ayyad, Marrakech B.P. 2410, Morocco; nadia.ouadi@gmail.com

⁴ Centre d'Etudes Spatiales de la Biosphère, Université de Toulouse, CNES, CNRS, IRD, UPS, 31400 Toulouse, France; Mehrez.Zribi@ird.fr (M.Z.); lionel.jarlan@cesbio.cnes.fr (L.J.)

⁵ Faculté des Sciences et Techniques, Université Cadi Ayyad, Marrakech B.P. 2410, Morocco; jamal.elfarkh@gmail.com (J.E.); aouade.ghizlane@gmail.com (G.A.)

* Correspondence: j.ezzahar@uca.ma or jamal.ezzahar@um6p.ma; Tel.: +212-5246-69155

Received: 19 October 2019; Accepted: 21 December 2019; Published: 24 December 2019

Abstract: The main objective of this work was to retrieve surface soil moisture (SSM) by using scattering models and a support vector machine (SVM) technique driven by backscattering coefficients obtained from Sentinel-1 satellite images acquired over bare agricultural soil in the Tensfit basin of Morocco. Two backscattering models were selected in this study due to their wide use in inversion procedures: the theoretical integral equation model (IEM) and the semi-empirical model (Oh). To this end, the sensitivity of the SAR backscattering coefficients at VV (σ_{vv}°) and VH (σ_{vh}°) polarizations to in situ soil moisture data were analyzed first. As expected, the results showed that over bare soil the σ_{vv}° was well correlated with SSM compared to the σ_{vh}° , which showed more dispersion with correlation coefficients values (r) of about 0.84 and 0.61 for the VV and VH polarizations, respectively. Afterwards, these values of σ_{vv}° were compared to those simulated by the backscatter models. It was found that IEM driven by the measured length correlation L slightly underestimated SAR backscatter coefficients compared to the Oh model with a bias of about -0.7 dB and -1.2 dB and a root mean square (RMSE) of about 1.1 dB and 1.5 dB for Oh and IEM models, respectively. However, the use of an optimal value of L significantly improved the bias of IEM, which became near to zero, and the RMSE decreased to 0.9 dB. Then, a classical inversion approach of σ_{vv}° observations based on backscattering model is compared to a data driven retrieval technic (SVM). By comparing the retrieved soil moisture against ground truth measurements, it was found that results of SVM were very encouraging and were close to those obtained by IEM model. The bias and RMSE were about 0.28 vol.% and 2.77 vol.% and -0.13 vol.% and 2.71 vol.% for SVM and IEM, respectively. However, by taking into account the difficulty of obtaining roughness parameter at large scale, it was concluded that SVM is still a useful tool to retrieve soil moisture, and therefore, can be fairly used to generate maps at such scales.

Keywords: soil moisture; synthetic aperture radar (SAR); Sentinel-1; semi-empirical and theoretical backscatter models; support vector machine; bare soil

1. Introduction

Estimates of the regional spatial-temporal variability of surface soil moisture (SSM) are in crucial need for better understanding the energy, water, and carbon exchanges at the land–atmosphere interface [1]. Indeed, surface soil moisture is a key state variable in various processes occurring on this interface, such as the partitioning of precipitation into infiltration and runoff [2] or of incoming solar radiation into sensible and latent heat [3–5]. Therefore, the involvement of accurate estimates of SSM in hydro-meteorological, climatic, and agricultural research and operations can be very useful for monitoring droughts [6], flood predictions [7,8], precipitations estimates [9,10], crop yield estimates [11], and weather forecasting [12]. For agricultural applications, an accurate description of soil moisture conditions at the field scale is of crucial importance before sowing and during the first stage of crop growth in order to determine the optimal sowing date and to schedule irrigation inputs. Conventionally, soil moisture can be accurately retrieved through in situ measurements, such as the time-domain reflectometry [13], cosmic-ray neutron method [14,15], and the gravimetric method [16]. However, for large scale applications, single measurements provided by these techniques have limited meaning because the moisture exhibits a strong spatio-temporal variability at several scales in relation to the heterogeneity of soil texture, topography, vegetation, and climate [17]. In practice, the straightforward solution for retrieving soil moisture at a large scale is to deploy a network of single measurements devices and then extrapolate the observations to provide spatial area-averaged values. However, due to high instrumental, logistic, and time costs, this solution cannot be implemented on an operational basis.

In this regard, the synthetic aperture radar systems (SAR) can be a valuable tool to provide fine spatial-temporal resolution for soil moisture estimation over agricultural areas [18–22]. Recently launched, Sentinel-1, which comprises two identical satellites (1A and 1B), potentially provides backscatter coefficient data at 20 m resolution every 3 days [23]. Considering bare soil, backscatter coefficient is closely related to soil moisture, mainly through its dielectric constant [18,24–26]. Thus, many backscattering models, varying in the degree of complexity, precision, and validity, have been developed for retrieving SSM over bare soil. These models can be categorized into three groups [21,27,28]: empirical, semi-empirical, and theoretical models. Based on a large number of experimental measurements and without any physical basis, purely empirical models were constructed to retrieve SSM from radar backscattering coefficient only under site specific conditions [29–32]. However, these models are generally non-transferable directly to others sites [27,29,33–37]. Semi-empirical models, such as the ones developed in [33,38], have been proposed as practical solutions to overcome the problem of the non-transferability. In spite of this advantage, the validity domain of these models is still limited to the range of data used for calibration [21]. Unlike empirical and semi-empirical models, physical models, such as the integral equation model (IEM) [39] can be fairly used in a wide range of configuration of acquisitions and of surface parameters [27,40]. Nevertheless, the main limiting factor to the use of theoretical models for surface soil moisture retrieval, particularly over large areas, appears to be the difficulty of describing the surface roughness [21,41]. Indeed, even with extensive in situ sampling of surface roughness, it remains difficult to characterize surface roughness at the field scale or larger due to the natural variability of the soil [42].

To surmount the limitations of empirical, semi-empirical, and physical models, machine-learning approaches provide an alternative tool to solve prediction problems based on an analysis of the data that characterizes the system under study with only a limited number of assumptions about the physical behavior of this system [43,44]. Among these approaches, one can cite the artificial neural network algorithm [45–47] and the support vector machine (SVM) technique. The latter, which is based on statistical learning theory, has been applied to a variety of themes, such as the inversion and classification problems, and has attracted the attention of many researchers due to their prediction accuracy and modeling conveniences [48–53]. Note that this technique which was first developed for the purpose of a classification problem (referred to as SVC) by [54], can be also used to perform regression tasks [48,55,56]. A version of a SVM for regression was first proposed in 1997 by [57] and

is called support vector regression (SVR). The main difference between both algorithms is that SVC predicts discrete categorical labels by involving one slack variable to each training data point in the optimization function, whereas SVR predicts continuous ordered variables using two slack variables for each training data point.

Concerning the application of SVR for the prediction of soil moisture, one can cite, for example, the work of [58], which demonstrated the potential of this technique compared to an artificial neural network (ANN) algorithm for predicting soil moisture for four and seven days in advance using meteorological variables. Additionally, [48], have used this technique for retrieving soil moisture from remote sensing data by combining backscatter from the Tropical Rainfall Measuring Mission (TRMM), and a normalized difference vegetation index (NDVI) from an advanced very high resolution radiometer (AVHRR), and they revealed that this technique performs better for soil moisture retrieval than the multivariate linear regression model (MLR). Recently, [59], confirmed the accuracy of the SVR model to predict soil moisture from soil temperature, NDVI, rainfall, and soil moisture observed the day before. To our knowledge, although SVR has been used in past studies for soil moisture retrieval, none of the studies have tested this algorithm with high resolution radar data. Moreover, there is no previous work that has evaluated the efficiency of SVR, driven specifically with Sentinel-1 data, on bare agricultural soils by comparison to more traditional techniques based on soil backscattering model inversion. In this research, the efficiency of SVR was evaluated against the soil backscattering model's inversion for soil moisture retrieval over bare agricultural soil using Sentinel-1 data. This paper is organized as follows: In Section 2, the study site and experimental setup are presented. Section 3 describes the backscattering models used to retrieve surface soil moisture. Section 4 contains a discussion about the results obtained. Finally, the conclusions are presented in the last section.

2. Study Site and Data Description

2.1. Study Site

The study took place in Sidi Rahal region, which is located 60 km east of Marrakech city, Morocco (Figure 1). The region is characterized by a semi-arid Mediterranean climate, with an average yearly precipitation in the order of 250 mm and an evaporative demand of around 1600 mm per year according to the FAO method [60,61]. The terrain is flat with elevation of 550 m above sea level, and the soil is characterized by a fine texture with 47% clay, 33% loam, and 18.5% sand. The agricultural fields, mainly irrigated and rainfall wheat crops [62], remained under bare soil conditions during the 2015–2016 agricultural season due to an unusual lack of precipitation in autumn 2015. In this study, only one experimental field of 1 ha, which is bounded by yellow in Figure 1, was selected to investigate the potential of backscatter models and SVR for retrieving surface soil moisture (SSM). The surface characteristics (SSM and surface roughness) were measured within this field. The red contour (Figure 1) which contains the experimental field was used to map SSM.

2.2. Ground Observations

At the center of the experimental field (Figure 1), a 2 m meteorological tower was installed in December 2013 in the frame work of the Joint International Laboratory TREMA (a French acronym for remote sensing and water resources in the semi-arid Mediterranean [61]). This tower is equipped with a set of sensors for measuring rainfall, global radiation, temperature, relative humidity, and wind speed at a half-hourly time step. The half hourly soil moisture (SM) is continuously measured using CS616 water content reflectometers (Campbell Scientific Ltd.) at different depths (5, 10, 20, 30, 50, 70 cm). These sensors were installed in a soil pit of 1 m depth located just below the meteorological tower. Two sensors were installed at 5 cm depth and only one sensor for the other depths. For comparison with the Sentinel-1 data, only the in situ measurements of the topsoil (5 cm) moisture content were used in this study. Data were extracted on the 42 dates when C-SAR Sentinel-1 images were available. Over the study region, these images were taken at 06:30 and 18:30; therefore, only

the average of the values collected between 06:00 and 19:00 was used. Additionally, the soil surface roughness was measured using a 1 m long needle-profilometer (Figure 2) and a sampling interval of 2 cm. Ten measurements were taken at several locations over the experimental field and were used to calculate the two roughness parameters' rmss (root mean squares)—surface height (s) and correlation length (L)—by using the mean of all experimental correlation functions. The processing of these data was done using a matlab software by providing all taken photos (as shown in (Figure 2)) and yielded averaged values of s and L over the experimental field.

2.3. SAR Satellite Images

Forty-two C-band SAR images acquired by the Sentinel-1 sensors between January and September 2016 over the study site were used in this work. Sentinel-1 comprises two identical satellites, 1A and 1B, which were launched in 2014 and 2016 respectively. With both satellites operating, the repeat cycle is 6 days. Table 1 lists the dates of the Sentinel-1 overpasses over our site during the study period. Over land, S1A and S1B operate in Interferometric Wide Swath mode, providing data at the cross polarization VH (vertical-horizontal) and co-polarization VV (vertical-vertical) mode with a 250 km swath at a 5 by 20 m spatial resolution. The incidence angle of S1A and S1B over the study site is about 40° . Level 1 S1A and S1B products were preprocessed using the Google Earth Engine cloud-based platform [63], in four steps: (i) thermal noise removal, (ii) radiometric calibration, (iii) terrain correction using SRTM (Shuttle Radar Topography Mission) DEM (Digital Elevation Model) at 30 m, and (iv) filtering speckle effects using the 5×5 refined Lee speckle filter described in [64,65]. Finally, the backscattering coefficients were then expressed in decibels (dB) using the formula:

$$\sigma^\circ (dB) = 10 \log_{10}(\sigma^\circ) \quad (1)$$

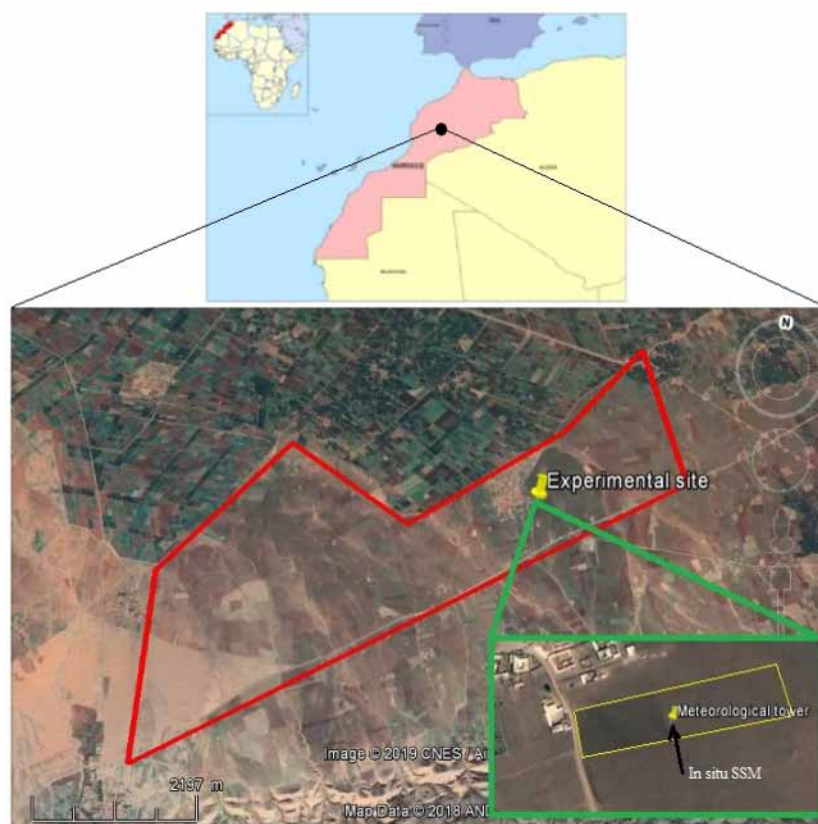


Figure 1. Location of Sidi Rahal site (east of Marrakech) in the Tensift basin, central Morocco. The experimental site (green contour), experimental field (yellow contour), positions of meteorological tower, in situ soil moisture measurements, and the areas of soil moisture (red contour) are marked.



Figure 2. Example of the needle-profilometer used in this study.

Table 1. Dates of the Sentinel-1 overpasses over our site during the study period. The Sentinel-1 images used for training or validation sets are also presented.

Overpasses Date (dd/mm/yyyy)	Training and Validation Datasets
07/01/2016	Training
15/01/2016	Validation
19/01/2016	Training
27/01/2016	Validation
31/01/2016	Training
08/02/2016	Validation
12/02/2016	Training
20/02/2016	Validation
24/02/2016	Training
03/03/2016	Validation
07/03/2016	Training
19/03/2016	Validation
27/03/2016	Training
31/03/2016	Validation
08/04/2016	Training
12/04/2016	Validation
20/04/2016	Training
24/04/2016	Validation
02/05/2016	Training
06/05/2016	Validation
14/05/2016	Training
18/05/2016	Validation
26/05/2016	Training
30/05/2016	Validation
07/06/2016	Training
11/06/2016	Validation
01/07/2016	Training
05/07/2016	Validation
13/07/2016	Training
17/07/2016	Validation
25/07/2016	Training
29/07/2016	Validation
06/08/2016	Training
10/08/2016	Validation
18/08/2016	Training
22/08/2016	Validation
30/08/2016	Training
03/09/2016	Validation
11/09/2016	Training
15/09/2016	Validation
23/09/2016	Training
27/09/2016	Validation

3. Backscattering Models

The relation between the soil surface moisture and SAR backscattering products is usually analyzed using backscattering models. Among numerous backscattering models, the most widely applied are the theoretical integral equation (IEM) and the semi-empirical Oh models. Herein, two versions of the physical integrated equation model were tested: the original one (IEM) and that modified recently by [66] *IEM_B* which uses an empirical model for estimating the correlation length l instead of using measured value. However, for the Oh model, only the version developed in 1992 was used. Indeed, several studies have showed that, in the C-band, this version simulates slightly better the backscattering in VV polarization than those developed later in 1994, 2002, and 2004 ([67,68]). In what follows, a description of both models is presented. As the Sentinel-1 provides only the backscattering coefficients in VH and VV polarizations, only the semi-empirical and theoretical expressions of these coefficients are provided.

3.1. The Semi-Empirical Oh Model

Based on existing theoretical scattering models, scatterometer measurements, and airborne SAR observations over a wide variety of bare soil surfaces, [38] developed a semi-empirical backscattering model in order to reproduce the radar backscattering coefficients in VH, VV, and HH polarizations (σ_{vh}^o , σ_{vv}^o and σ_{hh}^o). This model relates the co-polarized ratio $p(= \sigma_{hh}^o / \sigma_{vv}^o)$ and the cross-polarized ratio $q(= \sigma_{vh}^o / \sigma_{vv}^o)$ to radar wave incident angle (θ , in radians), wave number ($k = 2\pi/\lambda$ where λ is the wavelength), standard deviation of surface height ($Hrms$), correlation length (L), and soil moisture (m) or soil dielectric constant (ϵ_r). The empirical expressions of σ_{vh}^o , σ_{vv}^o are as follows:

$$\sigma_{vv}^o = g \cos^3 \theta \cdot [R_v + R_h] / \sqrt{p} \quad (2)$$

$$\sigma_{vh}^o = q \sigma_{vv}^o \quad (3)$$

where

$$q = 0.23(1 - \exp(-ks))\sqrt{R_o} \quad (4)$$

$$\sqrt{p} = 1 - \exp(-ks) \cdot (2\theta/\pi)^{[1/3R_o]} \quad (5)$$

$$g = 0.7 \left[1 - \exp \left(-0.65(ks)^{1.8} \right) \right]. \quad (6)$$

R_o , R_v , R_h denote the Fresnel coefficients given by the following expressions:

$$R_o = \left| \frac{1 - \sqrt{\epsilon_r}}{1 + \sqrt{\epsilon_r}} \right|^2, \quad R_v = \frac{\epsilon_r \cos \theta - \sqrt{\epsilon_r - \sin^2 \theta}}{(\epsilon_r \cos \theta - \sqrt{\epsilon_r - \sin^2 \theta})^2}, \quad R_h = \frac{\cos \theta - \sqrt{\epsilon_r - \sin^2 \theta}}{(\cos \theta - \sqrt{\epsilon_r - \sin^2 \theta})^2}. \quad (7)$$

3.2. The Physical Integral Equation Model (IEM)

The integral equation IEM is a theoretical backscattering model applicable to a wide range of roughness conditions [39]. The model solves the integral equations for the surface fields, taking into account the dielectric constant (ϵ_r), the standard deviation of surface height ($Hrms$), the form of the correlation function, and the correlation length (L); and the sensor parameters, such as the incidence angle (θ), the polarization (pq with $p, q = h$ or v), and the radar wave number. The model is valid with $kHrms \leq 3$ which is commonly encountered for most agricultural surfaces. The backscatter coefficient of the surface contribution is expressed as:

$$\begin{aligned} \sigma_{pp}^{\circ} = & \frac{k}{2} |f_{pp}|^2 e^{-4k^2 H_{rms}^2 \cos^2 \theta} \sum_{n=1}^{+\infty} \frac{(4k^2 H_{rms}^2 \cos^2 \theta)^n}{n!} W^{(n)}(2k \sin \theta, 0) + \\ & \frac{k}{2} Re(f_{pp}^* F_{pp}) e^{-3k^2 H_{rms}^2 \cos^2 \theta} \sum_{n=1}^{+\infty} \frac{(4k^2 H_{rms}^2 \cos^2 \theta)^n}{n!} W^{(n)}(2k \sin \theta, 0) + \\ & \frac{k}{8} |F_{pp}|^2 e^{-2k^2 H_{rms}^2 \cos^2 \theta} \sum_{n=1}^{+\infty} \frac{(4k^2 H_{rms}^2 \cos^2 \theta)^n}{n!} W^{(n)}(2k \sin \theta, 0). \end{aligned} \quad (8)$$

At cross polarization, the backscattering coefficient is as follows:

$$\begin{aligned} \sigma_{hv}^{\circ} = & \frac{k}{16\pi} e^{-2k^2 H_{rms}^2 \cos^2 \theta} \sum_{n=1}^{+\infty} \sum_{m=1}^{+\infty} \frac{(4k^2 H_{rms}^2 \cos^2 \theta)^{n+m}}{n!m!} \\ & \iint [|F_{hv}(u, v)|^2 + F_{hv}^*(-u, -v)] W^m(u + k \sin \theta, v) dudv, \end{aligned} \quad (9)$$

where:

$$f_{hh} = \frac{-2R_h}{\cos \theta}; \quad f_{vv} = \frac{-2R_v}{\cos \theta} \quad (10)$$

$$F_{hh} = 2 \frac{\sin^2 \theta}{\cos \theta} \left[4R_h - \left(1 - \frac{1}{\epsilon_r} \right) (1 + R_h)^2 \right] \quad (11)$$

$$F_{vv} = 2 \frac{\sin^2 \theta}{\cos \theta} \left[\left(1 - \frac{\epsilon_r \cos^2 \theta}{\mu_r \epsilon_r - \sin^2 \theta} \right) (1 - R_v)^2 + \left(1 - \frac{1}{\epsilon_r} \right) (1 + R_v)^2 \right] \quad (12)$$

$$F_{hv}(u, v) = \frac{uv}{k \cos \theta} \left[\frac{8R^2}{\sqrt{k^2 - u^2 - v^2}} + \frac{-2 + 6R^2 + \frac{(1+R)^2}{\epsilon_r} + \epsilon_r(1 - R)^2}{\sqrt{\epsilon_r k^2 - u^2 - v^2}} \right]. \quad (13)$$

$$R = \frac{R_v - R_h}{2} \quad (14)$$

ϵ_r : dielectric constant obtained using the Hallikainen empirical model (Reference).

μ_r : relative permittivity.

Re : real part of the complex number.

f_{pp}^* : conjugate of the complex number f_{pp} .

$W^{(n)}$ is the Fourier transform of the nth power of the surface correlation $\rho(x, y)$ function:

$$W^{(n)}(a, b) = \frac{1}{2\pi} \iint \rho^n(x, y) e^{-i(ax+by)} dx dy. \quad (15)$$

The expression of the correlation function $\rho(x, y)$ is related to the nature of its distribution and can be defined for one-dimensional roughness profiles as:

$$\rho(x, y) = \begin{cases} e^{-\frac{x}{l}} & : \text{exponential dsitribution} \\ e^{-\left(\frac{x}{l}\right)^2} & : \text{gaussian dsitribution} \end{cases}. \quad (16)$$

In order to evaluate the accuracies of different approaches used in this study, the root mean square (RMSE) and bias are calculated according to the following equations (ys and yo are the simulated and observed values, respectively):

$$RMSE = \sqrt{\frac{1}{n} \sum_{k=1}^n (y_{s_k} - y_{o_k})^2} \quad (17)$$

$$Bias = \frac{1}{n} \sum_{k=1}^n (y_{s_k} - y_{o_k}) \quad (18)$$

4. Results and Discussion

In this study, the Sentinel-1 backscattering coefficient was averaged on the experimental field surrounding the meteorological station (yellow contour in Figure 1). Additionally, the local measurement of the soil moisture measured near to the meteorological tower (see ground observations section) was assumed to be representative for the experimental field due the absence of the vegetation and irrigation. As mentioned before, only an average of the values collected between 6 h p.m./a.m. and 7 p.m./a.m. was used. Additionally, the roughness characteristics, including rms surface height (s) and correlation length (L), were averaged using sampling taken at different locations on the experimental field. Overall, this section is organized as follows: firstly, the empirical relation between the Sentinel-1 backscattering coefficient and the top soil moisture is investigated. Secondly, the potential of Oh and IEM models for simulating the backscattering coefficient, using the measured soil moisture and soil surface roughness, is evaluated based on the comparison with Sentinel-1 backscattering coefficients. Thirdly, the surface soil moisture over the experimental field is retrieved using two approaches: non-linear regression (support vector regression—SVR) and the inversion of Oh and IEM models. Both approaches were driven by Sentinel-1 backscattering coefficient. Likewise, the measured soil roughness was used as input for the inverse algorithm of Oh and IEM. Finally, the SVR algorithm was used to map surface soil moisture using only the averaged backscattering coefficient derived from Sentinel-1 and extracted over the mapping area (red color, Figure 1)

4.1. Relation between Radar Backscattering Coefficient and Soil Moisture

The high spatial resolution of the Sentinel-1 data (10 m) made it possible to analyze the radar signal according to surface parameters such as the soil moisture and roughness at the plot scale. In the current study, the analysis was focused only on the soil moisture, assuming that the roughness effect on radar signal was approximately the same for all of the experiment period. Indeed, the soil was not ploughed up due to an unusual lack of precipitation in autumn/winter 2015. Additionally, the sensitivity of radar signal to soil moisture SM is strongly affected by the incidence angle. Indeed, previous studies, using C-band data, have pointed out that this sensitivity is greater at the low to medium incidence angles (20°–37°) and decreases with increasing incidence angle [29,30,69]. However, as mentioned before, the incidence angle of S1 over the study site was about 40°, and therefore, its sensitivity could not be analyzed in this work.

As reported in several research studies realized over bare agricultural areas [70–73], the Sentinel-1 backscattering coefficients σ_{vv}° and σ_{vh}° were related to measured soil moisture using linear regression (Figure 3). During this study, the soil moisture values varied between 4 and 25 vol.% and the values of σ_{vh}° and σ_{vv}° ranged from −21.61 dB to −25.05 dB (~−3.43 dB) and from −11.97 dB to −16.73 dB (~−4.76 dB), respectively. By analyzing this figure, it can be clearly seen that the Sentinel-1 radar at VV polarization is significantly correlated with the measured soil moisture compared to the VH polarization which showed more dispersion. The correlation coefficients (r) were about 0.84 and 0.61 for the VV and VH polarizations, respectively. Additionally, the sensitivity of the radar backscatter to measured soil moisture was estimated as 0.23 and 0.11 dB/vol.% for VV and VH polarizations, respectively. Thus, an increase in moisture content of approximately 5% generates an increase in σ_{vv}° of approximately 1.15 dB and only 0.55 dB in σ_{vh}° .

Overall, the results obtained over the experimental period, including all soil moisture data measured, are consistent with the radar sensitivity over bare soils pointed out by several previous studies in the case of data acquired in C-band [70,71,73–76], and confirm that the VV polarization is more suitable for quantifying the soil contribution. By contrast, the VH has been shown to be more related to the vegetation contribution to the radar backscatter since VH is more sensitive to the vegetation volume scattering mechanism, due to the depolarization effect by vegetation-volume-scattering, which mainly

depends on the vegetation characteristics [73,77–79]. Therefore, based on this result, only the VV polarization is used throughout the rest of the manuscript.

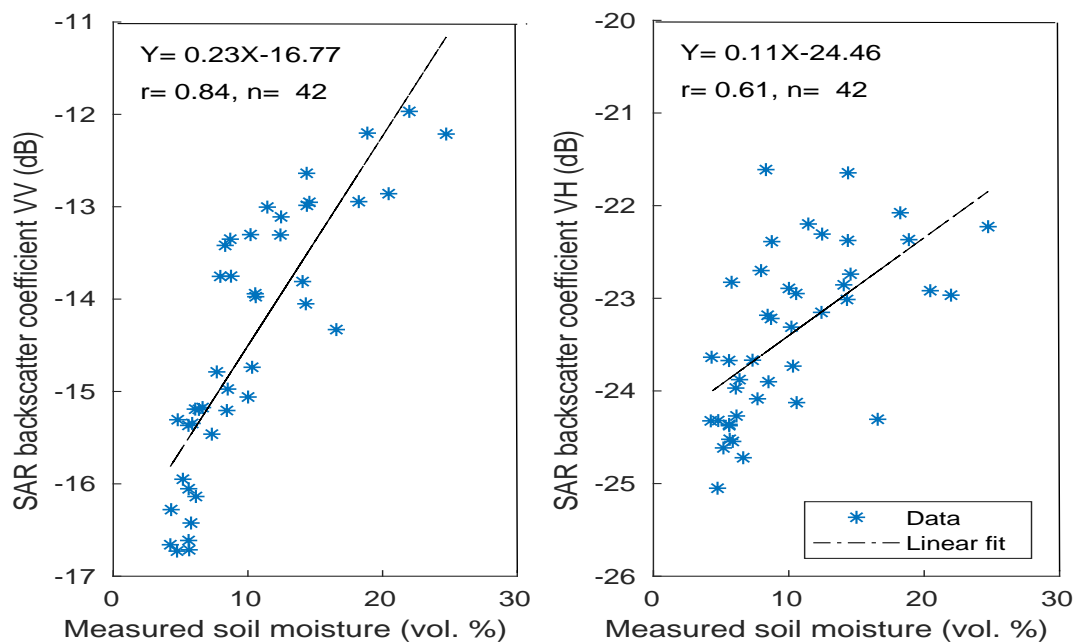


Figure 3. The relationship between SAR on-board Sentinel-1 backscatter coefficient and measured soil moisture at 5 cm for both polarizations: VV (left) and VH (right). The linear regression lines are also plotted.

4.2. Evaluation of the Oh and IEM Models

In this study, the backscatter coefficients of Oh and IEM models were simulated only at VV polarization due to its high sensitivity to soil moisture, as shown above (Section 4.1). The performance of scattering models in simulating the backscatter coefficient is evaluated throughout the manuscript using the mean difference between the simulated and Sentinel-1 backscattering coefficients (bias) across all dates, the root mean square errors, and correlation coefficients (r). Figure 4 shows the comparison between backscatter coefficients derived from the Sentinel-1 and those simulated by Oh model where n represents the number of backscatter coefficients data. Based on the analysis of statistical results, one can notice clearly that in spite of its semi-empirical behavior, the Oh model correctly simulates the radar signal with a difference between Sentinel-1 and simulated data of -0.7 dB. Besides, RMSE and r are of 1.1 dB and 0.85, respectively. This finding is in good accordance with the previous studies which have reported the ability of Oh model for simulating the radar in VV polarization, particularly in the C-band. For instance, [80] have showed that, in C-band, the Oh model gave closer backscatter coefficients to the observed values from a truck-mounted scatterometer with a r of about 0.88. Likewise, [81] have compared the output of Oh model at VV polarization with those acquired from the airborne synthetic aperture radar (AIRSAR) in the C-band and they revealed that the semi-empirical model gave a reasonable result with a RMSE of about 1.1 dB. Recently, by combining several synthetic aperture radars such as ASAR, ERS, SIR-C, RADARSAT, and AIRSAR, another study realized by [68] has proven the potential of the version of Oh model we used for simulating the backscattering coefficient. Their results showed that Oh model developed in 1992 had the best fit of the backscattering coefficients in VV polarization compared to the 1994, 2002, and 2004 versions. The difference between SAR and simulated data was about 0.4 dB and the RMSE of about 2.3 dB.

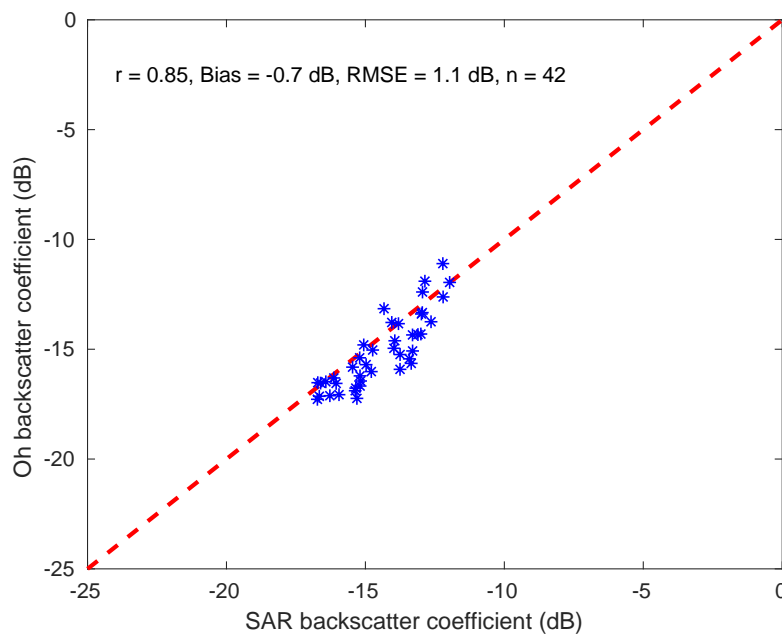


Figure 4. Comparison between backscattering coefficients derived from Sentinel-1 images and those simulated by the Oh 1992 model at VV polarization.

Figure 5 compares the Sentinel-1 and simulated backscatter coefficients for the original IEM using the in situ measurement of the correlation length L and the exponential distribution of the correlation function. It is worth noting that the IEM slightly underestimates the backscatter coefficients compared to the Oh model. The mean difference between Sentinel-1 and simulated data was about -1.2 dB, an underestimation 0.5 dB more than the Oh model. Additionally, the RMSE was about 1.5 dB, larger than the value given by Oh model by about 0.4 dB, while the r values were more or less similar (about 0.84 for IEM). It is interesting to note that the use of Gaussian correlation yielded a poor correlation between Sentinel-1 and simulated backscatter coefficients (not shown). The simulated backscatter coefficients were very low compared to the Sentinel-1 ones and their average was around -39 dB, while that of Sentinel-1 was about -14.5 dB. This result was expected due to the nature of the study site, which is characterized by low value of surface roughness [22,67]. This is in accordance with several previous studies which have found that, for agricultural surfaces, the exponential function provides the best match between predicted and SAR backscatters [82–85]. Generally speaking, in spite of the slight underestimation, one can state that the simulations of IEM by using the measured L are very satisfying with respect to what have been reported in previous works [20,67,80,81,86]. However, measuring the correlation length is a problematic task because of its dependence on the profile length, as well as the standard deviation of surface height (H_{rms}) [86], and thus its is considered as the most difficult parameter to be measured at the field with a good accuracy. In the same vein, several studies have reported that the discrepancies between backscattering coefficients simulated by IEM and those measured by SAR sensors are mainly related to the value of L measured [87,88]. The uncertainties in this important key input can probably generate error in soil moisture retrieval from backscatter coefficients by inverting IEM. Indeed, [89] have stated that an error magnitude of 2 dB induces an imprecision of 7% on soil moisture retrieval. Therefore, in order to improve the simulations by IEM, L was replaced by an optimal one (L_{opt}), as described in [68], which was obtained by forcing the IEM until a good agreement was reached between simulations and SAR data. To this end, the data were equally subdivided into a calibration and validation sets. The calibration dataset (training dataset in Table 1) was used to optimize L_{opt} , while the validation dataset (validation dataset in Table 1) was used to validate the modified IEM using the new calibrated empirical model of L_{opt} . The choice of these data was made as follows: one of two images was used for calibration and another for validation.

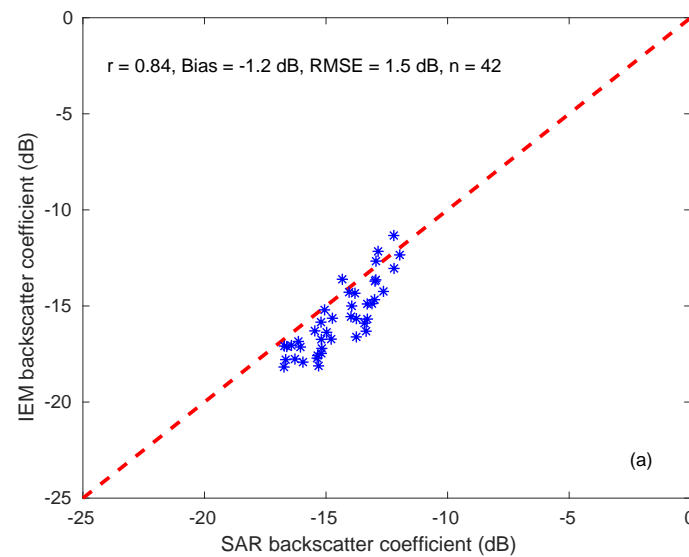


Figure 5. Comparison between backscattering coefficients derived from Sentinel-1 images and those simulated by the IEM model at VV polarization using measured L .

Figure 6 displays the Sentinel-1 and simulated backscatter coefficients using the modified (L_{opt}) and original (measured L) versions of IEM for the validation dataset. Results show that the new simulations by the modified IEM provide more accurate results compared to those of the original version by selecting only a validation dataset. The later yielded values of bias, RMSE, and r of about -1.5 dB, 1.7 dB, and 0.92 . RMSE decreases from 1.7 dB to 0.9 dB and the slight underestimation was clearly eliminated since the bias was near to zero (about -0.4 dB) with a similar value of r . These findings can be considered fairly good results and are in accordance with previous works. Recently, using several bands, including C-band, [68], has proven that with the use of L_{opt} , the modified IEM improved significantly backscatter coefficients in comparison to the original version in VV polarization, with a difference between SAR data and model simulations approximately equal to $+0.1$ dB, RMSE was about 2 dB. Additionally, by comparing with the Oh model for the same dataset, it can be noticed that the modified version ploughed improves slightly the simulated backscatter coefficients.

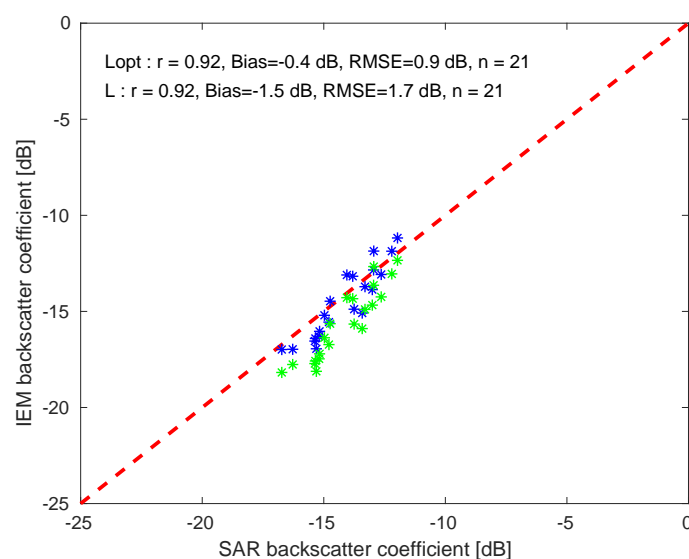


Figure 6. Comparison between backscattering coefficients derived from Sentinel-1 images and those simulated by the IEM model at VV polarization using measured L (green color) and optimal L_{opt} (blue color) correlation length for the validation data ($n = 21$).

4.3. Soil Moisture Inversion

In this section, the potential of Oh and IEM models, and the use of the SVR algorithm for predicting the soil moisture from the Sentinel-1 backscattering coefficient data over bare soil is investigated. Validation for the proposed algorithms is based on a comparison against ground-truth measurements of soil moisture ranging from dry to wet over the tested site. As of the calibration of the correlation length, to run the SVR algorithm, the data were subdivided into a training and a validation datasets (see table 1). As cited before, the choice of these data is made as follows: one of two images was used for calibration and another for validation. In order to correctly evaluate SVR against the inversed algorithms of Oh and IEM models, only the validation dataset is used in this section.

Figures 7 and 8 show the scatter plot of measured and retrieved soil moisture from radar backscattering coefficient using Oh and IEM (modified version by using the measured $hrms$ and $Lopt$) models, respectively. Overall, the results show that the retrieved soil moisture by inverting Oh model slightly over-estimates the ground-truth measurements with a bias of about 2.45 vol.%. Besides, the RMSE and r were about 3.19 vol.% and 0.92, respectively. Although some discrepancies can be observed, this result is similar to those reported in previous studies such as [38,90–92]. However, for the IEM model using the $Lopt$, it was found that the retrieved soil moisture matched well with the ground-truth measurements compared to Oh model, although a small under-estimation can be noticed when the soil is very wet (soil moisture is larger than 20%). RMSE, bias, and r were approximately 2.4 vol.%, 0.71 vol.%, and 0.91, respectively. It is worth mentioning that the comparison between the measured and retrieved soil moisture from IEM model using the measured L yielded less performance than that obtained by Oh and IEM (using the $Lopt$) models (not shown). The values of RMSE and bias were approximately 4.47 vol.% and 3.99 vol.%, respectively. Similar results have been achieved by [40], who have stated that the use of adjusted L instead of the measured one improves, considerably, the soil moisture retrieval with a significant decrease of RMSE from 0.13 to 0.05 vol.%. Therefore, based on its physical basis behavior compared to semi-empirical models, it can be concluded that this finding may demonstrate that it is probably the input parameters that result in poor performance of the IEM model rather than the model itself [93]. It should be noted that the adjustment of L is based on the assumption that $hrms$ can be accurately measured in the field [87,94]. In [40], they obtained little additional improvement in the soil moisture retrieval by adjusting $hrms$ and L simultaneously. Nonetheless, they revealed that the adjusting of both parameters can cause a large influence on the accuracy of soil moisture retrieval, particularly in wetter conditions.

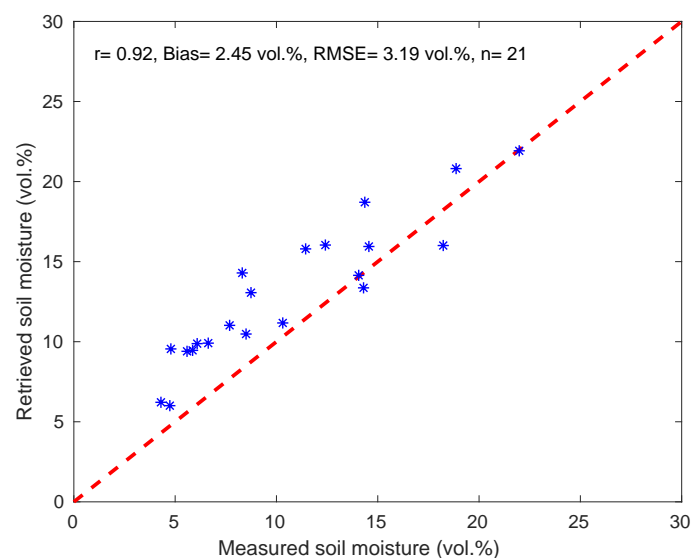


Figure 7. Comparison between retrieved soil moisture using Oh model and ground-truth measurements.

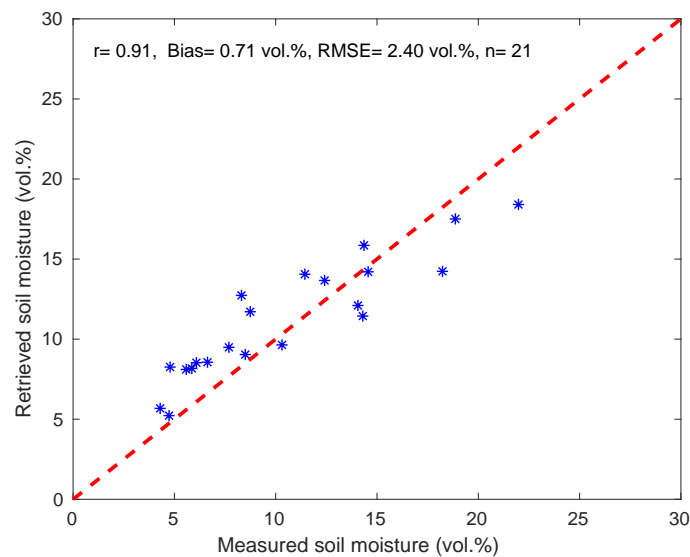


Figure 8. Comparison between retrieved soil moisture using IEM model and ground-truth measurements.

As the ultimate goal of this work was to evaluate SVR based mainly on statistical learning against semi-empirical and theoretical soil backscattering models, SVR was also driven by Sentinel-1 backscattering coefficient data for retrieving soil moisture retrieval. Usually, machine learning methods used to retrieve soil moisture were trained with backscattering coefficient data generated from backscattering models and validated using radar data [47,95]. However, the error associated with the use of these models can be directly translated into an error in soil moisture retrieval. In this specific study, the training dataset was used to build a regression SVR model (MDL), whereas the validation dataset was used to compare the performance of the predicted model with a calibrated MDL as an input. It should be noted that, based on the selected method for the training and validation sets, the range of soil moisture variation was almost similar for both datasets (from dry to wet conditions). Additionally, the surface roughness was constant during the study period because the soil was not plowed due to the late of rainfall. Figure 9 displays the comparison between measured and retrieved soil moisture using SVR algorithm driven by Sentinel-1 backscattering coefficient data. A good correlation between measured and retrieved soil moisture is detected, with values of r , RMSE, and bias of about 0.89, 2.72 vol.%, and -0.13 vol.%, showing that this approach is a powerful algorithm for retrieving soil moisture. The obtained performance in the statistical metrics, which is probably related to the fact that soil roughness conditions were very specific, may be lessened under conditions of greater roughness. These statistical results are close to those found by the IEM model using the adjusted L (Figure 8). Additionally, as shown by IEM model, the SVR algorithm underestimates the soil moisture slightly for values larger than 15 vol.%. This can be related to the limit of training dataset within this range of soil moisture variation. As a matter of fact, as with all machine learning methods, SVR needs numerous training dataset in order to correctly build the regression model.

In spite of the improvement obtained by reducing the input parameters of IEM by using an optimal value of correlation length, the retrieved of regional soil moisture through backscatter models still requires spatial measurements of root-mean-square (RMS) height, which is not an easy task particularly over heterogeneous areas. Therefore, it can be concluded that the SVM technique which uses only the radar backscatter data can be a good tool for large-scale soil moisture monitoring. For this purpose, the SVR was tested to map soil moisture over a large bare soil area, which limits the study site. Figure 10 displays two maps of soil moisture obtained by using SAR images acquired on 27/03/2016 (three days after rainfall event) and 25/07/2016 (dry conditions). As expected, the values of soil moisture obtained for wet conditions were higher than those for dry conditions. Indeed, the mean moisture level was approximately equal to 12 vol.% for wet conditions and was about 6 vol.% for dry

conditions. Overall, the values of soil moisture over bare soils are within the limits of measurements values. Under dry conditions, it can be seen that within some pixels, the values are very high. This due to the existence of some fruits inside or in front of the building near to the experimental field. Likewise, there is small fields of irrigated crops (alfalfa for example) within the mapping area and a fruit orchard which can increase the soil moisture in the summer. This result confirms clearly the potential of SVR technique for mapping soil moisture over bare soil areas, at least under our conditions.

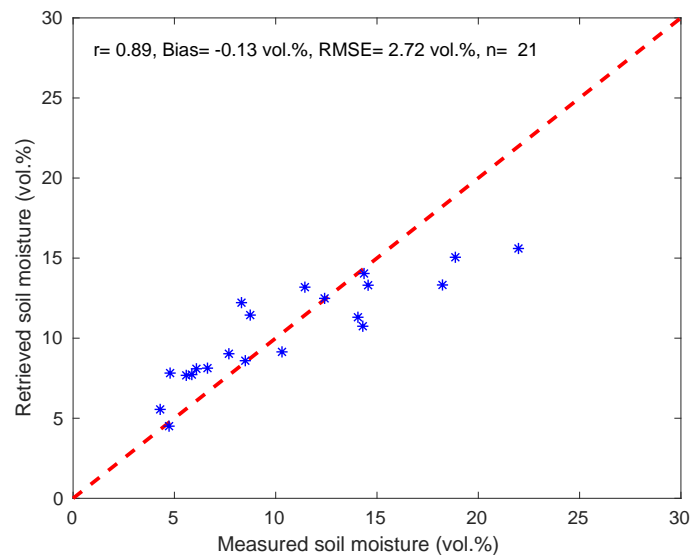


Figure 9. Comparison between retrieved soil moisture using support vector machine and ground-truth measurements.

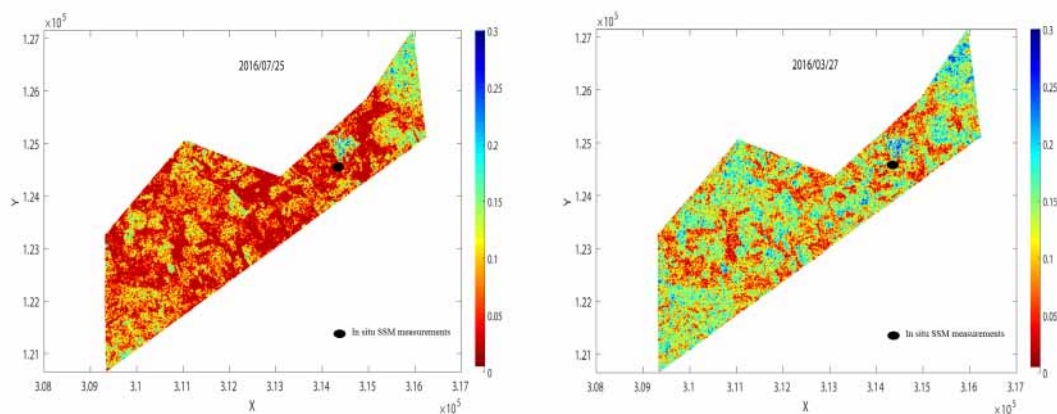


Figure 10. Mapping of soil moisture (vol.%) using support vector machine: dry (left) and wet (right) conditions.

5. Conclusions

This study investigated the capability of using Sentinel-1 backscatter data to retrieve surface soil moisture over bare agricultural soil in Tensift basin of Morocco. This retrieval was made through the application of inversion algorithms based on the theoretical integral equation model (IEM) and the semi-empirical model (Oh) or directly by using support vector regression technique. A field of 1 ha was selected to investigate the potential of these algorithms. Within this field, measurements of soil moisture and surface roughness were made. In a first step, a sensitivity analysis of the Sentinel-1 backscatter coefficients at both VV and VH polarizations to ground truth measurements of soil moisture was done. It was found that the linear regression obtained for the VV polarization presented less dispersion than VH. Overall, this sensitivity was estimated as 0.23 and 0.11 dB for VV and VH polarizations,

respectively. Therefore, only the backscattering coefficients at VV polarization were used to retrieve soil moisture in this study. Afterwards, and before discussing the inversion procedure, the backscattering coefficients estimated by Oh and IEM models were compared with Sentinel-1 backscatter data. This comparison showed that the driven IEM model by an optimal value of correlation length instead of a measured one improved the simulated backscatter coefficients and even gave slightly better results compared to the Oh model.

In the second step, the soil moisture was retrieved from Sentinel-1 backscattering coefficient data by inverting Oh and IEM models, and by the use of SVR. The comparison against ground-truth data showed that IEM and SVR gave acceptable results with values of RMSE of about 2.72 vol.% and 2.4 vol.% respectively, while the Oh model showed more discrepancies (RMSE = 3.19 vol.%) with an overestimation of the soil moisture (2.45 vol.%). However, in spite of the improvement obtained by reducing the input parameters of IEM by using an optimal value of correlation length, the retrieval of regional soil moisture through backscatter models still requires spatial measurements of root-mean-square (RMS) height, which is not an easy task, particularly over heterogeneous areas.

In parallel, the SVR algorithm gave a comparable result to the IEM model for the retrieval of soil moisture. The acceptable statistical metrics obtained with SVR are probably related to the fact that roughness conditions over bare agricultural soils are very specific. Indeed, roughness conditions there were almost unchanging because the soil was not plowed due to the late rainfall. It is likely that the application of our approach to other surfaces such as fallows would exhibit a drastic drop of performances. Finally, it can be concluded that the SVR technique, which uses only the radar backscatter data, can be a good tool for large-scale soil moisture monitoring over bare agricultural soils, which is of crucial importance to determining the optimal sowing date and to schedule irrigation inputs. Additionally, the result of this work can be fairly used to validate the products provided by passive microwave sensors, such as SMOS or SMAP, using disaggregation algorithms. The current research can be used as an alternative to the computationally expensive and data intensive physical model. As far as short term prospects go, we intend to apply this technique to retrieve soil moisture over wheat crops and compare the results to those from backscattering models by combining the water cloud model and IEM model—which simulate the vegetation and soil contributions, respectively. In addition, the values obtained will be used as in conjunction with the land surface temperature from sentinel-3 in the new thermal-based two-source energy balance (TSEB-SM) developed by [96] to map the evapotranspiration.

Author Contributions: J.E. (Jamal Ezzahar), L.J., and M.Z. conceived the original idea of this work and analyzed the data. J.E. (Jamal Ezzahar) wrote the paper. N.O. provided the data. J.E. (Jamal Elfarkh) contributed to the mapping of soil moisture. G.A., S.K., S.E.-R., and A.C. revised the paper.

Funding: Initial set up and maintenance of the field instrumentation were funded by the Joint International Laboratory TREMA <https://www.lmi-trema.ma>. This research was supported by PHC Toubkal TBK/18/61, TOSCA MOCTAR, H2020 RISE ACCWA (grant agreement number: 823965), and ERANETMED03-62 CHAAMS projects.

Acknowledgments: The BEST fellowship program from Institut de Recherche pour le Développement (IRD) is fully acknowledged.

Conflicts of Interest: The authors declare no conflict of interest.

References

1. Zeng, L.; Hu, S.; Xiang, D.; Zhang, X.; Li, D.; Li, L.; Zhang, T. Multilayer Soil Moisture Mapping at a Regional Scale from Multisource Data via a Machine Learning Method. *Remote Sens.* **2019**, *11*, 284. [[CrossRef](#)]
2. Seneviratne, S.I.; Corti, T.; Davin, E.L.; Hirschi, M.; Jaeger, E.B.; Lehner, I.; Orlowsky, B.; Teuling, A.J. Investigating soil moisture-climate interactions in a changing climate: A review. *Earth-Sci. Rev.* **2010**, *99*, 125–161. [[CrossRef](#)]
3. Daly, E.; Porporato, A. A review of soil moisture dynamics: From rainfall infiltration to ecosystem response. *Environ. Eng. Sci.* **2005**, *22*, 9–24. [[CrossRef](#)]

4. Koster, R.D.; Dirmeyer, P.A.; Guo, Z.; Bonan, G.; Chan, E.; Cox, P.; Gordonet, C.T.; Kanaeal, S.; Kowalczyk, E.; Lawrence, D.; et al. Regions of strong coupling between soil moisture and precipitation. *Science* **2004**, *305*, 1138–1140. [[CrossRef](#)]
5. Western, A.W.; Grayson, R.B.; Blöschl, G. Scaling of soil moisture: A hydrologic perspective. *Annu. Rev. Earth Planet. Sci.* **2002**, *30*, 149–180. [[CrossRef](#)]
6. Bolten, J.D.; Crow, W.T.; Zhan, X.; Jackson, T.J.; Reynolds, C.A. Evaluating the utility of remotely sensed soil moisture retrievals for operational agricultural drought monitoring. *IEEE J. Sel. Top. Appl. Earth Obs. Remote Sens.* **2010**, *3*, 57–66. [[CrossRef](#)]
7. Wanders, N.; Karssenbergh, D.; Roo, A.D.; De Jong, S.; Bierkens, M. The suitability of remotely sensed soil moisture for improving operational flood forecasting. *Hydrol. Earth Syst. Sci.* **2014**, *18*, 2343–2357. [[CrossRef](#)]
8. Alvarez-Garreton, C.; Ryu, D.; Western, A.; Su, C.-H.; Crow, W.; Robertson, D.; Leahy, C. Improving operational flood ensemble prediction by the assimilation of satellite soil moisture: comparison between lumped and semi-distributed schemes. *Hydrol. Earth Syst. Sci.* **2015**, *19*, 1659–1676. [[CrossRef](#)]
9. Wanders, N.; Pan, M.; Wood, E. Correction of real-time satellite precipitation with multi-sensor satellite observations of land surface variables. *Remote Sens. Environ.* **2015**, *160*, 206–221. [[CrossRef](#)]
10. Zhan, W.; Pan, M.; Wanders, N.; Wood, E. Correction of real-time satellite precipitation with satellite soil moisture observations. *Earth Syst. Sci.* **2015**, *19*, 4275–4291. [[CrossRef](#)]
11. Manzoni, S.; Vico, G.; Palmroth, S.; Porporato, A.; Katul, G. Optimization of stomatal conductance for maximum carbon gain under dynamic soil moisture. *Adv. Water Resour.* **2013**, *62*, 90–105. [[CrossRef](#)]
12. Drusch, M.; Scipal, K.; De Rosnay, P.; Balsamo, G.; Andersson, E.; Bougeault, P.; Viterbo, P. Towards a Kalman Filter based soil moisture analysis system for the operational ECMWF Integrated Forecast System. *Geophys. Res. Lett.* **2009**, *36*, L10401. [[CrossRef](#)]
13. Noborio, K. Measurement of soil water content and electrical conductivity by time domain reflectometry: A review. *Comput. Electron. Agric.* **2001**, *31*, 213–237. [[CrossRef](#)]
14. Zreda, M.; Shuttleworth, W.J.; Zeng, X.; Zweck, C.; Desilets, D.; Franz, T.; Rosolem, R. COSMOS: The COsmic-ray Soil Moisture Observing System. *Hydrol. Earth Syst. Sci.* **2012**, *16*, 4079–4099. [[CrossRef](#)]
15. Heidbüchel, I.; Güntner, A.; Blume, T. Use of cosmic-ray neutron sensors for soil moisture monitoring in forests. *Earth Syst. Sci.* **2016**, *20*, 1269–1288. [[CrossRef](#)]
16. Reynolds, S.G. The gravimetric method of soil moisture determination part I: A study of equipment and methodological problems. *J. Hydrol.* **1970**, *11*, 258–273. [[CrossRef](#)]
17. Kong, X.; Dorling, S.; Smith, R. Soil moisture modelling and validation at an agricultural site in Norfolk using the Met Office surface exchange scheme (MOSES). *Meteorol. Appl.* **2011**, *18*, 18–27. [[CrossRef](#)]
18. Das, K.; Paul, P.K. Present status of soil moisture estimation by microwave remote sensing. *Cogent Geosci.* **2015**, *1*, 1084669. [[CrossRef](#)]
19. Boisvert, J.B.; Pultz, T.J.; Brown, R.J.; Brisco, B. Potential of Synthetic Aperture Radar for Large-Scale Soil Moisture Monitoring: A Review. *Can. J. Remote Sens.* **1996**, *22*, 2–13. [[CrossRef](#)]
20. Van Oevelen, P.J.; Hoekman, D.H. Radar Backscatter Inversion Techniques for Estimation of Surface Soil Moisture: EFEDA-Spain and HAPEX-Sahel Case Studies. *IEEE Trans. Geosci. Remote Sens.* **1999**, *37*, 113–123. [[CrossRef](#)]
21. Karthikeyan, L.; Pan, M.; Wanders, N.; Kumar, D.N.; Wood, E.F. Four decades of microwave satellite soil moisture observations: Part 1. A review of retrieval algorithms. *Adv. Water Res.* **2017**, *109*, 106–120. [[CrossRef](#)]
22. Barrett, B.W.; Dwyer, E.; Whelan, P. Soil Moisture Retrieval from Active Spaceborne Microwave Observations: An Evaluation of Current Techniques. *Remote Sens.* **2009**, *1*, 210–242. [[CrossRef](#)]
23. Torres, R.; Snoeij, P.; Geudtner, D.; Bibby, D.; Davidson, M.; Attema, E.; Potin, P.; Rommen, B.; Floury, N.; Brown, M.; et al. GMES Sentinel-1 mission. *Remote Sens. Environ.* **2012**, *120*, 9–24. [[CrossRef](#)]
24. Prakash, R.; Singh, D.; Pathak, N.P. A fusion approach to retrieve soil moisture with SAR and optical data. *IEEE J. Sel. Top. Appl. Earth Obs. Remote Sens.* **2012**, *5*, 196–206. [[CrossRef](#)]
25. Schmugge, T.J.; Jackson, T.J.; McKim, H.L. Survey of methods for soil moisture determination. *Water Resour. Res.* **1980**, *16*, 961–979. [[CrossRef](#)]
26. Amazirh, A.; Merlin, O.; Er-Raki, S.; Gao, Q.; Rivalland, V.; Malbeteau, Y.; Khabba, S.; Escorihuela, M.J. Retrieving surface soil moisture at high spatio-temporal resolution from a synergy between Sentinel-1 radar and Landsat thermal data: A study case over bare soil. *Remote Sens. Environ.* **2018**, *201*, 321–337. [[CrossRef](#)]

27. Kornelsen, K.C.; Coulibaly, P. Advances in soil moisture retrieval from synthetic aperture radar and hydrological applications. *J. Hydrol.* **2013**, *476*, 460–489. [[CrossRef](#)]
28. Petropoulos, G.P.; Ireland, G.; Barrett, B. Surface soil moisture retrievals from remote sensing: Current status, products and future trends. *Phys. Chem. Earth* **2015**, *83*, 36–56. [[CrossRef](#)]
29. Le Hegarat Mascle, S.; Zribi, M.; Alem, F.; Weisse, A.; Loumagne, C. Soil moisture estimation from ERS/SAR data: Toward an operational methodology. *IEEE Trans. Geosci. Remote Sens.* **2002**, *40*, 2647–2658. [[CrossRef](#)]
30. Quesney, A.; Le Hégarat-Masclé, S.; Taconet, O.; Vidal-Madjar, D.; Wigneron, J.P.; Loumagne, C.; Normand, M. Estimation of watershed soil moisture index from ERS/SAR data. *Remote Sens. Environ.* **2000**, *72*, 290–303. [[CrossRef](#)]
31. Wang, J.R.; Hsu, A.; Shi, J.C.; O'Neill, P.E.; Engman, E.T. A comparison of soil moisture retrieval models using SIR-C measurements over the Little Washita River watershed. *Remote Sens. Environ.* **1997**, *59*, 308–320. [[CrossRef](#)]
32. Zribi, M.; Baghdadi, N.; Holah, N.; Fafin, O. New methodology for soil surface moisture estimation and its application to ENVISAT-ASAR multi-incidence data inversion. *Remote Sens. Environ.* **2005**, *96*, 485–496. [[CrossRef](#)]
33. Dubois, P.C.; van Zyl, J.; Engman, T. Measuring soil moisture with imaging radars. *IEEE Trans. Geosci. Remote Sens.* **2005**, *33*, 915–926. [[CrossRef](#)]
34. Moran, M.S.; Hymer, D.C.; Qi, J.G.; Sano, E.E. Soil moisture evaluation using multi-temporal synthetic aperture radar (SAR) in semiarid rangeland. *Agric. For. Meteorol.* **2000**, *105*, 69–80. [[CrossRef](#)]
35. Baghdadi, N.; Aubert, M.; Cerdan, O.; Franchistéguy, L.; Viel, C.; Eric, M.; Zribi, M.; Desprats, J.F. Operational mapping of soil moisture using synthetic aperture radar data: application to the Touch basin (France). *Sensors* **2007**, *7*, 2458–2483. [[CrossRef](#)] [[PubMed](#)]
36. Baghdadi, N.; Cerdan, O.; Zribi, M.; Auzet, V.; Darboux, F.; El Hajj, M.; Kheir, R.B. Operational performance of current synthetic aperture radar sensors in mapping soil surface characteristics in agricultural environments: application to hydrological and erosion modelling. *Hydrol. Process.* **2008**, *22*, 9–20. [[CrossRef](#)]
37. Verhoest, N.E.; Lievens, H.; Wagner, W.; Álvarez-Mozos, J.; Moran, M.S.; Mattia, F. On the soil roughness parameterization problem in soil moisture retrieval of bare surfaces from synthetic aperture radar. *Sensors* **2008**, *8*, 4213–4248. [[CrossRef](#)]
38. Oh, Y.; Sarabandi, K.; Ulaby, F.T. An Empirical Model and an Inversion Technique for Radar Scattering from Bare Soil Surfaces. *IEEE Trans. Geosci. Remote Sens.* **1992**, *30*, 370–381. [[CrossRef](#)]
39. Fung, A.K.; Li, Z.; Chen, K.S. Backscattering from a randomly rough dielectric surface. *IEEE Trans. Geosci. Remote Sens.* **1992**, *30*, 356–369. [[CrossRef](#)]
40. Thoma, D.P.; Moran, M.S.; Bryant, R.; Rahman, M.; Holifield-Collins, C.D. Skirvin, S. Comparison of four models to determine surface soil moisture from C-band radar imagery in a sparsely vegetated semiarid landscape. *Water Resour. Res.* **2006**, *42*, W01418. [[CrossRef](#)]
41. Barrett, B.W.; Petropoulos, G.P. Satellite Remote sensing of Surface Soil Moisture. In *Remote Sensing of Energy Fluxes Soil Moisture Content*; Petropoulos, G.P., Ed.; Taylor and Francis Group: Abingdon, UK, 2017; pp. 85–120. ISBN 9781138077577.
42. Srivastava, H.S.; Patel, P.; Sharma, Y.; Navalgund, R.R. Retrieval of surface roughness using multi-polarized ENVISAT ASAR data. *Geocarto Int.* **2008**, *23*, 67–77. [[CrossRef](#)]
43. Khalil, A.; Almasri, M.N.; Mckee, M.; Kaluarachchi, J.J. Applicability of statistical learning algorithms in groundwater quality modeling. *Water Resour. Res.* **2005**, *41*, 147–150. [[CrossRef](#)]
44. Solomatine, D.P.; Shrestha, D.L. A novel method to estimate model uncertainty using machine learning techniques. *Water Resour. Res.* **2009**, *45*, W00B11. [[CrossRef](#)]
45. Baghdadi, N.; Cresson, R.; El Hajj, M.; Ludwig, R.; La Jeunesse, I. Estimation of soil parameters over bare agriculture areas from C-band polarimetric SAR data using neural networks. *Hydrol. Earth Syst. Sci.* **2012**, *16*, 1607–1621. [[CrossRef](#)]
46. El Hajj, M.; Baghdadi, N.; Zribi, M.; Bazzi, H. Synergic use of Sentinel-1 and Sentinel-2 images for operational soil moisture mapping at high spatial resolution over agricultural areas. *Remote Sens.* **2017**, *9*, 1292. [[CrossRef](#)]
47. Mirsoleimani, H.R.; Sahebi, M.R.; Baghdadi, N.; El Hajj, M. Bare Soil Surface Moisture Retrieval from Sentinel-1 SAR Data Based on the Calibrated IEM and Dubois Models Using Neural Networks. *Sensors* **2019**, *19*, 3209. [[CrossRef](#)]

48. Ahmad, S.; Kalra, A.; Stephen, H. Estimating soil moisture using remote sensing data: A machine learning approach. *Adv. Water Resour.* **2010**, *33*, 69–80. [[CrossRef](#)]
49. Lin, G.F.; Chen, G.R.; Wu, M.C.; Chou, Y.C. Effective forecasting of hourly typhoon rainfall using support vector machines. *Water. Resour. Res.* **2009**, *45*, W08440. [[CrossRef](#)]
50. Kalra, A.; Ahmad, S. Using oceanic–atmospheric oscillations for long lead time streamflow forecasting. *Water. Resour. Res.* **2009**, *45*, W03413. [[CrossRef](#)]
51. Liong, S.Y.; Sivapragasam, C. Flood stage forecasting with support vector machines. *J. Am. Water Resour. Assoc.* **2002**, *38*, 173–186. [[CrossRef](#)]
52. Asefa, T.; Kemblowski, M.; McKee, M.; Khalil, A. Multi-time scale stream flow predictions: the support vector machines approach. *J. Hydrol.* **2006**, *318*, 7–16. [[CrossRef](#)]
53. Pasolli, L.; Notarnicola, C.; Bruzzone, L. Estimating Soil Moisture with the Support Vector Regression Technique. *IEEE Geosci. Remote Sens. Lett.* **2011**, *8*, 1080–1084. [[CrossRef](#)]
54. Vapnik, V. *The Nature of Statistical Learning Theory*; Springer: New York, NY, USA, 1995; p. 122, ISBN 978-1-4757-3264-1.
55. Cortes, C.; Vapnik, V.N. Support-vector networks. *Mach. Learn.* **1995**, *20*, 273–297. [[CrossRef](#)]
56. Kecman, V. Learning and Soft Computing. In *A Bradford Book*; The MIT Press: Cambridge, MA, USA, 2001; 541p.
57. Vapnik, V.; Golowich, S.; Smola, A. Support Vector Method for Function Approximation, Regression Estimation, and Signal Processing. In *Neural Information Processing Systems*; Mozer, M., Jordan, M., Petsche, T., Eds.; MIT Press: Cambridge, UK, 1997; Volume 9, pp. 281–287.
58. Gill, M.K.; Asefa, T.; Kemblowski, M.; McKee, M. Soil moisture prediction using support vector machines. *J. Am. Water Resour. Assoc.* **2006**, *42*, 1033–1046. [[CrossRef](#)]
59. Lee, D.; Kim, G.; Lee, K.E.T. Soil moisture prediction using a support vector regression. *J. Korean Data Inf. Sci. Soc.* **2013**, *14*, 401–408. [[CrossRef](#)]
60. Allen, R.G.; Pereira, L.S.; Raes, D.; Smith, M. *Crop Evapotranspiration—Guidelines for Computing Crop Water Requirements, Irrigation and Drain*; Paper No. 56; FAO: Rome, Italy, 1998; 300p.
61. Jarlan, L.; Khabba, S.; Er-Raki, S.; Le Page, M.; Hanich, L.; Fakir, Y.; Merlin, O.; Mangiarotti, S.; Gascoin, S.; Ezzahar, J.; et al. Remote sensing of water resources in semi-arid Mediterranean basins: The Joint International Laboratory TREMA. *Int. J. Remote Sens.* **2015**, *36*, 4879–4917. [[CrossRef](#)]
62. Ezzahar, J.; Chehbouni, A.; Er-Raki, S.; Hanich, L. Combining a Large Aperture Scintillometer and estimates of available energy to derive evapotranspiration over several agricultural fields in semi-arid regions. *Plant Biosyst.* **2009**, *143*, 209–221. [[CrossRef](#)]
63. Gorelick, N.; Hancher, M.; Dixon, M.; Ilyushchenko, S.; Thau, D.; Moore, R. Google Earth Engine: Planetary-scale geospatial analysis for everyone. *Remote Sens. Environ.* **2017**, *202*, 18–27. [[CrossRef](#)]
64. Lee, J.S.; Grunes, M.R.; de Grandi, G. Polarimetric SAR speckle filtering and its implication for classification. *IEEE Trans. Geosci. Remote Sens.* **1999**, *37*, 2363–2373. [[CrossRef](#)]
65. Lee, J.S.; Jurkevich, L.; Dewaele, P.; Wambacq, P.; Oosterlinck, A. Speckle filtering of synthetic aperture radar images: A review. *Remote Sens. Rev.* **1994**, *8*, 313–340. [[CrossRef](#)]
66. Baghdadi, N.; Chaaya, J.A.; Zribi, M. Semiempirical calibration of the integral equation model for SAR data in C-band and cross polarization using radar images and field measurements. *IEEE Geosci. Remote Sens. Lett.* **2011**, *8*, 14–18. [[CrossRef](#)]
67. Baghdadi, N.; Mehrez, Z. Evaluation of radar backscatter models IEM, OH and Dubois using experimental observations. *Int. J. Remote Sens.* **2006**, *27*, 3831–3852. [[CrossRef](#)]
68. Choker, M.; Baghdadi, N.; Zribi, M.; El Hajj, M.; Paloscia, S.; Verhoest, N.; Lievens, H.; Mattia, F. Evaluation of the Oh, Dubois and IEM models using large dataset of SAR signal and experimental soil measurements. *Water* **2017**, *9*, 38. [[CrossRef](#)]
69. Holah, N.; Baghdadi, N.; Zribi, M.; Bruand, A.; King, C. Potential of ASAR/ENVISAT for the characterization of soil surface parameters over bare agricultural fields. *Remote Sens. Environ.* **2005**, *96*, 78–86. [[CrossRef](#)]
70. Baghdadi, N.; Holah, N.; Zribi, M. Soil moisture estimation using multi-incidence and multi-polarization ASAR SAR data. *Int. J. Remote Sens.* **2006**, *27*, 1907–1920. [[CrossRef](#)]
71. Le Morvan, A.; Zribi, M.; Baghdadi, N.; Chanzy, A. Soil Moisture Profile Effect on Radar Signal Measurement. *Sensors* **2008**, *8*, 256–270. [[CrossRef](#)]

72. Aubert, M.; Baghdadi, N.; Zribi, M.; Douaoui, A.; Loumagne, C.; Baup, F.; El Hajj, M.; Garrigues, S. Analysis of TerraSAR-X data sensitivity to bare soil moisture, roughness, composition and soil crust. *Remote Sens. Environ.* **2011**, *115*, 1801–1810. [[CrossRef](#)]
73. Eweys, O.A.; Escorihuela, M.J.; Villar, J.M.; Er-Raki, S.; Amazirh, A.; Olivera, L.; Jarlan, L.; Khabba, S.; Merlin, O. Disaggregation of SMOS Soil Moisture to 100 m Resolution Using MODIS Optical/Thermal and Sentinel-1 Radar Data: Evaluation over a Bare Soil Site in Morocco. *Remote Sens.* **2017**, *9*, 1155. [[CrossRef](#)]
74. Dabrowska-Zielinska, D.; Musial, J.; Malinska, A.; Budzynska, M.; Gurdak, R.; Kiryla, W.; Bartold, M.; Grzybowski, P. Soil Moisture in the Biebrza Wetlands Retrieved from Sentinel-1 Imagery. *Remote Sens.* **2018**, *10*, 1979. [[CrossRef](#)]
75. Baghdadi, N.; El Hajj, M.; Zribi, M.; Bousbih, S. Calibration of the Water Cloud Model at C-Band for Winter Crop Fields and Grasslands. *Remote Sens.* **2017**, *9*, 969. [[CrossRef](#)]
76. Bousbih, S.; Zribi, M.; Lili-Chabaane, Z.; Baghdadi, N.; El Hajj, M.; Gao, Q.; Mougenot, B. Potential of Sentinel-1 Radar Data for the Assessment of Soil and Cereal Cover Parameters. *Sensors* **2017**, *17*, 2617. [[CrossRef](#)] [[PubMed](#)]
77. Chauhan, S.; Srivastava, H.S. Comparative evaluation of the sensitivity of multi-polarised Sar and optical data for various land cover. *Int. J. Adv. Remote Sens. GIS Geogr.* **2016**, *4*, 1–14.
78. Gao, Q.; Zribi, M.; Escorihuela, M.; Baghdadi, N. Synergetic use of Sentinel-1 and Sentinel-2 data for soil moisture mapping at 100 m resolution. *Sensors* **2017**, *17*, 1966. [[CrossRef](#)] [[PubMed](#)]
79. Karjalainen, M.; Harri, K.; Hyypä, J.; Laurila, H.; Kuittinen, R. The use of Envisat alternating polarization Sar images in agricultural monitoring in comparison with Radarsat-1 Sar images. In Proceedings of the ISPRS Congress, Istanbul, Turkey, 12–23 July 2004.
80. Boisvert, J.B.; Gwyn, Q.H.J.; Chanzy, A.; Major, D.J.; Brisco, B.; Brown, R.J. Effect of surface soil moisture gradients on modelling radar backscattering from bare fields. *Int. J. Remote Sens.* **1997**, *18*, 153–170. [[CrossRef](#)]
81. MirMazloumi, S.M.; Sahebi, M.R. Assessment of Different Backscattering Models for Bare Soil Surface Parameters Estimation from SAR Data in band C, L and P. *Eur. J. Remote Sens.* **2016**, *49*, 261–278. [[CrossRef](#)]
82. Baghdadi, N.; Gherboudj, I.; Zribi, M.; Sahebi, M.; King, C.; Bonn, F. Semi-empirical calibration of the IEM backscattering model using radar images and moisture and roughness field measurements. *Int. J. Remote Sens.* **2004**, *25*, 3593–3623. [[CrossRef](#)]
83. Baghdadi, N.; Zribi, M.; Paloscia, S.; Verhoest, N.E.; Lievens, H.; Baup, F.; Mattia, F. Semi-empirical calibration of the integral equation model for co-polarized L-band backscattering. *Remote Sens.* **2015**, *7*, 13626–13640. [[CrossRef](#)]
84. Panciera, R.; Tanase, M.A.; Lowell, K.; Walker, J.P. Evaluation of IEM, Dubois, and Oh Radar Backscatter Models Using Airborne L-Band SAR. *IEEE Trans. Geosci. Remote Sens.* **2014**, *52*, 4966–4979. [[CrossRef](#)]
85. Bai, X.; He, B.; Li, X.; Zeng, J.; Wang, X.; Wang, Z.; Zeng, Y.; Su, Z. First Assessment of Sentinel-1A Data for Surface Soil Moisture Estimations Using a Coupled Water Cloud Model and Advanced Integral Equation Model over the Tibetan Plateau. *Remote Sens.* **2017**, *9*, 714. [[CrossRef](#)]
86. Ghafouri, A.; Amini, J.; Dehmollaian, M.; Kavooosi, M.A. Better Estimated IEM Input Parameters Using Random Fractal Geometry Applied on Multi-Frequency SAR Data. *Remote Sens.* **2017**, *9*, 445. [[CrossRef](#)]
87. Baghdadi, N.; King, C.; Chanzy, A.; Wigneron, J.P. An empirical calibration of the integral equation model based on SAR data, soil moisture and surface roughness measurement over bare soils. *Int. J. Remote Sens.* **2002**, *23*, 4325–4340. [[CrossRef](#)]
88. Baghdadi, N.; Paillou, P.; Grandjean, G.; Dubois, P.; Davidson, M. Relationship between profile length and roughness variables for natural surfaces. *Int. J. Remote Sens.* **2000**, *21*, 3375–3381. [[CrossRef](#)]
89. Merzouki, A.; Bannari, A.; Teillet, P.M.; King, D.J. Statistical properties of soil moisture images derived from Radarsat-1 SAR data. *Int. J. Remote Sens.* **2011**, *32*, 5443–5460. [[CrossRef](#)]
90. Eweys, O.A.; Elwan, A.A.; Borham, T.I. Retrieving topsoil moisture using RADARSAT-2 data, a novel approach applied at the east of the Netherlands. *J. Hydrol.* **2017**, *555*, 670–682. [[CrossRef](#)]
91. Hajnsek, I.; Jagdhuber, T.; Schön, H.; Papathanassiou, K.P. Potential of estimating soil moisture under vegetation cover by means of PolSAR. *IEEE Trans. Geosci. Remote Sens.* **2009**, *47*, 442–454. [[CrossRef](#)]
92. Gherboudj, I.; Magagi, R.; Berg, A.A.; Toth, B. Soil moisture retrieval over agricultural fields from multi-polarized and multi-angular RADARSAT-2 SAR data. *Remote Sens. Environ.* **2011**, *151*, 33–43. [[CrossRef](#)]

93. Rahman, M.M.; Moran, M.S.; Thoma, D.P.; Bryant, R.; Holifield Collins, C.D.; Jackson, T.; Orr, B.J.; Tischler, M. Mapping surface roughness and soil moisture using multi-angle radar imagery without ancillary data. *Remote Sens. Environ.* **2008**, *112*, 391–402. [[CrossRef](#)]
94. Verhoest, N.E.C.; Hoeben, R.; De Troch, F.P.; Troch, P.A. Soil moisture inversion from ERS and SIR-C imagery at the Zwalm catchment, Belgium. *IEEE Proc. Int. Geosci. Remote Sens. Symp.* **2000**, *5*, 2041–2043. [[CrossRef](#)]
95. El Hajj, M.; Baghdadi, N.; Zribi, M.; Belaud, G.; Cheviron, B.; Courault, D.; Charron, F. Soil moisture retrieval over irrigated grassland using X-band SAR data. *Remote Sens. Environ.* **2016**, *176*, 202–218. [[CrossRef](#)]
96. Ait Hssaine, B.; Merlin, O.; Ezzahar, J.; Ojha, N.; Er-Raki, S.; Khabba, S. An evapotranspiration model self-calibrated from remotely sensed surface soil moisture, land surface temperature and vegetation cover fraction: application to disaggregated SMOS and MODIS data. *Hydrol. Earth Syst. Sci.* (in revision). [[CrossRef](#)]



© 2019 by the authors. Licensee MDPI, Basel, Switzerland. This article is an open access article distributed under the terms and conditions of the Creative Commons Attribution (CC BY) license (<http://creativecommons.org/licenses/by/4.0/>).